Materials Science and Engineering A 416 (2006) 155–160

www.elsevier.com/locate/msea

Investigation of hydrogen sulfide stress corrosion cracking of PH 13-8 Mo stainless steel

L.W. Tsay [a,*], M.Y. Chi [a], H.R. Chen [b], C. Chen [b]

[a] *Institute of Materials Engineering, National Taiwan Ocean University, Keelung 202, ROC, Taiwan*
[b] *Department of Materials Science and Engineering, National Taiwan University, Taipei 106, ROC, Taiwan*

Received in revised form 21 September 2005; accepted 5 October 2005

Abstract

Slow displacement rate tensile tests were carried out in a saturated H_2S solution to investigate the effect of hydrogen embrittlement on notched tensile strength (NTS) and fracture characteristics of aged PH 13-8 Mo stainless steel. Hydrogen diffusivity, permeation flux and apparent hydrogen solubility were determined by an electrochemical permeation method, and correlated with the inherent microstructure of the specimens. All aged specimens were susceptible to sulfide stress corrosion cracking (SSCC) to various degrees. Similar permeation properties were observed for specimens aged in the temperature range of 427 °C (800 °F) to 538 °C (1000 °F). In contrast, much lower diffusivity and hydrogen flux together with a higher solubility of hydrogen were found for the specimen aged at 593 °C (1100 °F), i.e. the H1100 specimen. For specimens aged below 538 °C, the resembling permeation behavior led to the same level of susceptibility to hydrogen embrittlement as revealed by their NTS losses. Whereas, the H1100 specimen with low diffusivity and hydrogen flux implied that less hydrogen could be transferred to the strained region, resulting in a low NTS loss. The trapping of hydrogen in the matrix enhanced the quasi-cleavage fracture for specimens aged below 538 °C in the notched tensile test. On the other hand, hydrogen tended to trap at grain boundary austenite of the H1100 specimen, resulting in an intergranular separation under the test.

Keywords: PH 13-8 Mo stainless steel; Sulfide stress corrosion cracking; Notched tensile strength; Hydrogen embrittlement; Hydrogen permeation

1. Introduction

PH 13-8 Mo is a precipitation-hardened martensitic stainless steel, which combines high strength with moderate corrosion resistance. After cooling from solution temperature, the microstructure of the steel comprises of large irregular blocky units of lath martensite [1]. Aging in the temperature range between 450 and 575 °C leads to finely distributed β-NiAl particles which are spherical and remain fully coherent with the matrix even after the over-aging treatment [1,2]. A certain amount of reverted austenite is also found to nucleate on grain boundaries for PH 13-8 Mo aged at 468 °C (875 °F) [3] and martensite lath boundaries for over-aged specimens [2]. The volume fraction of reverted austenite increases rapidly with increasing the aging time or temperature [1–4]. Moreover, the strength and hardness decrease, while the ductility and impact toughness of the alloy increase with increasing the aging temperature [2].

Similar to other high strength steels, PH 13-8 Mo stainless steel exhibits a marked decrease in both strength and ductility as a result of hydrogen charging [5]. The initiation fracture toughness (J_i) of this alloy is severely embrittled by hydrogen, but the severity depends on the hydrogen concentration [6]. Crack growth of PH 13-8 Mo in hydrogen sulfide solution is mostly transgranular in all heat-treated conditions [2]. The lack of intergranular fracture is probably due to its much lower impurity content segregated to prior austenite grain boundaries of the material [2]. However, mixed mode fracture (intergranular and brittle transgranular fracture) might occur in hydrogen charged PH 13-8 Mo stainless steel [5,7]. The susceptibility to hydrogen embrittlement of the alloy decreases as the aging temperature is increased, indicating the dependence of microstructures [3]. In the solution-treated condition, PH 13-8 Mo can be more resistant to sulfide stress corrosion cracking (SSCC) than other high strength steels owing to the presence of a small amount of retained austenite in the structure [8]. The substantial improvement in SSCC is obtained for the alloy aged at 620 °C and above due to the formation of considerable amounts of reverted austenite in the structure [7].

* Corresponding author. Tel.: +886 2 24622192x6405; fax: +886 2 24625324.
E-mail address: b0186@mail.ntou.edu.tw (L.W. Tsay).

0921-5093/$ – see front matter © 2005 Elsevier B.V. All rights reserved.
doi:10.1016/j.msea.2005.10.021

The purpose of this study was to investigate the effect of SSCC on notched tensile strength (NTS) and fracture characteristics of aged PH 13-8 Mo stainless steel under slow displacement-rate tensile tests. The susceptibility to hydrogen embrittlement of various specimens was accessed by comparing the NTS in air with that in H_2S-saturated solution. The degradation of notched tensile strength (NTS) and related fracture characteristics of specimens were examined. The influence of microstructure and hydrogen permeation properties on the hydrogen embrittlement susceptibility was performed on these specimens. Hydrogen diffusivity and solubility as determined by an electrochemical method in conjunction with microstructure were used to explain SSCC behavior of distinct specimens.

2. Material and experimental procedures

The chemical composition (in weight percent) of PH 13-8 Mo stainless steel used in this investigation was 12.56Cr, 8.11Ni, 2.12Mo, 0.05C, 0.04Si, 0.05Mn, 0.006P, 0.003S, 0.006N, 1.07Al, and balance Fe. The alloy was solution-treated in an inert environment at 930 °C (1700 °F) for 40 min and then air-cooled to room temperature. The aging treatments were performed at 427 °C (800 °F), 482 °C (900 °F), 538 °C (1000 °F) and 593 °C (1100 °F) for 4 h, the associated specimens were designated as H800, H900, H1000 and H1100 specimens, respectively.

The dimensions of smooth and notched tensile specimens utilized in this study are shown in Fig. 1. Ordinary tensile tests of smooth specimens (Fig. 1(a)) with a gauge length of 12.5 mm were performed at room temperature in laboratory air under the strain rates of $5 \times 10^{-4}\,s^{-1}$. The double-edge notched specimens (Fig. 1(b)), having a notch radius of about 100 μm, were made by using an electrode-discharge wire cutter. The effect of hydrogen embrittlement on NTS was evaluated by installing the specimen in a Teflon chamber with saturated H_2S solution

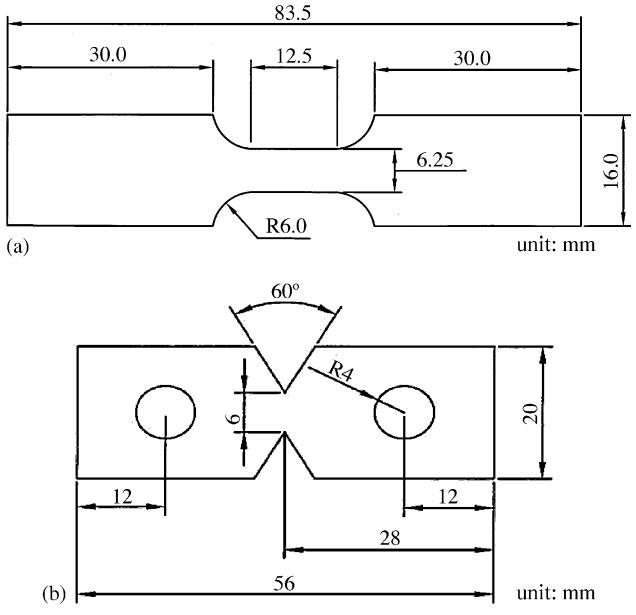

Fig. 1. Schematic diagrams showing the dimensions of the (a) smooth and (b) notched tensile specimens.

(NACE TM-01-77-86), and tested at constant crosshead displacement rates of 0.0075 and 0.0015 mm/min. The results were the average of at least three specimens for each testing condition. The susceptibility to hydrogen embrittlement can be expressed in the percentage loss in NTS after hydrogen-charging as follow:

$$\text{NTS loss (\%)} = \frac{\text{NTS (in air)} - \text{NTS (in } H_2\text{ S)}}{\text{NTS (in air)}}$$

Electrochemical permeation technique originally developed by Devanathan and Stachurski [9] was employed to determine the hydrogen permeation behavior of various specimens. The specimen after grinding and polishing was electroplated with Pd of 0.2 μm thick on hydrogen exit side. The exposed surface area (1 cm^2) of the specimen (0.25 mm thick) also acted as working electrode. The cathodic (hydrogen entry) side was galvanostatically polarized and charged at a constant current density (20 mA/cm^2) in 0.1 N NaOH added with 20 mg As_2O_3/l as hydrogen promoter. The anodic (hydrogen exit) side was held at a constant potential of +200 mV versus saturated calomel electrode in 0.1 N NaOH at room temperature. Solutions on both sides of the cell were deoxygenated by continuously purging N_2 bubbles. The potentiostatic current gave a direct measurement of the hydrogen flow rate, and hydrogen permeation transient was recorded continuously on a computer. The effective hydrogen diffusivity (D_{eff}), permeation flux ($J_\infty L$, where J_∞ is the steady state flux of hydrogen and L is the specimen thickness), and the apparent hydrogen solubility (C_{app}) were determined according to the equations given in the paper [9].

Tensile-fracture specimens were examined by a Hitachi S4100 scanning electron microscope (SEM), with emphasis on the crack initiation sites and regions showing changes in fracture appearance. Thin foil specimens were prepared by a standard jet-polisher, and then examined with a JEOL-2000 EX transmission electron microscope (TEM).

3. Results and discussion

3.1. Microstructural observations

TEM micrographs of specimens aged at various temperatures are shown in Fig. 2. The microstructures of H800 and H900 specimens consisted of ultra-fine precipitates within lath martensite matrix. Meanwhile, less austenite was present mainly at martensite lath boundaries in the H800 specimen as shown in Fig. 2(a) and (b). In case of the H1100 specimen, a homogeneous distribution of very fine precipitates together with the presence of reverted austenite in the island form within the matrix was observed (Fig. 2(c) and (d)). The size and amount of austenite increase greatly in the H1100 specimen as compared with other aged specimens. It was also noted that some austenite not only grew laterally along the prior austenite grain boundaries but also extended into another grain in the H1100 specimen.

It has been reported that the microstructure of PH 13-8 Mo aged at 468° C (875° F) consists of coherent β-NiAl precipitates in the martensite matrix with a high dislocation density [3]. In addition, the transformation of martensite to stable austenite

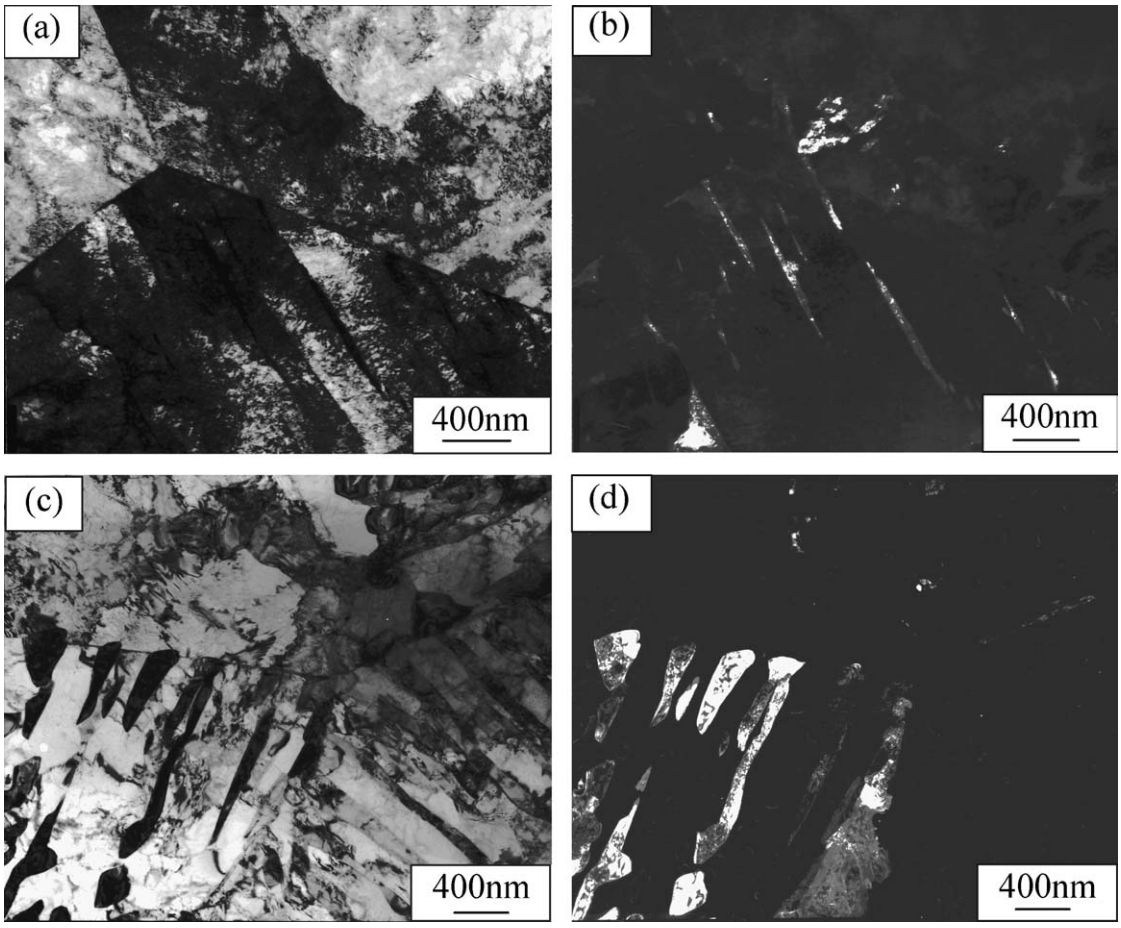

Fig. 2. TEM micrographs showing the (a) bright field, (b) dark field image of the H800 specimen, (c) bright field and (d) dark field image of the H1100 specimen. Note that dark field images were using austenite reflections.

was found for aged specimens and the content was about 5.0%, 6.5%, and 7.5% for H875, H950 and H1025 specimens [3], respectively. In the present work, austenite was found mainly on the martensite lath boundaries and less on prior austenite grain boundaries. Hydrogen is known to trap mainly at austenite/ferrite interfaces and the hydrogen solubility is also higher in austenite than that in ferrite [10]. As revealed by the microstructures, the H800 specimen consisted of the least, while the H1100 specimen possessed the most amounts of strong traps among the specimens. The influence of various traps on the cracking susceptibility in aged specimens was discussed in the following sections.

3.2. Tensile tests

Table 1 listed the tensile properties of aged specimens which were tested at room temperature in air. The hardness of the H800 specimen was H_{RC} 41.4, which was slightly higher than H_{RC} 38.2 of the H1100 specimen, but lower than H_{RC} 46.6 of the H1000 and H_{RC} 46.8 of the H900 specimens. According to the tensile strength, specimens aged in the temperature range of 427–593° C could be roughly divided into two groups, e.g. 1450 and 1200 MPa levels. H900 and H1000 specimens had a similar tensile strength level of 1450 MPa, whereas, H800 and H1100 specimens had the strength at approximately 1200 MPa. The lower strength of H800 and H1100 specimens could be attributed to the formation of ultra-fine coherent particles in the former and the existence of a significant amount of reverted austenite in the latter. Precipitation of a small amount of carbides and reverted austenite has been reported to deteriorate the yield strength of over-aged PH 13-8 Mo steel [11].

The NTS values of PH 13-8 Mo steel tested in air and saturated H_2S solution at two displacement rates are shown in Fig. 3. The presence of notch caused somewhat notch strengthening (compared with the data in Table 1) of the specimens in air. H900 and H1000 specimens had higher NTS than H800 and H1100 specimens in air, which were consistent with the result of smooth specimens. Testing in the saturated H_2S solution and at a displacement rate of 0.0075 mm/min, the H1100

Table 1
Tensile results of aged specimens tested at room temperature in air

	H800	H900	H1000	H1100
UTS (MPa)	1263 ± 15	1486 ± 12	1460 ± 10	1180 ± 15
YS (MPa)	1051 ± 20	1356 ± 16	1328 ± 22	1050 ± 20
EL (%)	12.5	12.0	12.0	16.0
Hardness (H_{RC})	41.1	46.8	46.7	38.2

UTS: ultimate tensile strength; YS: yield strength; EL: elongation.

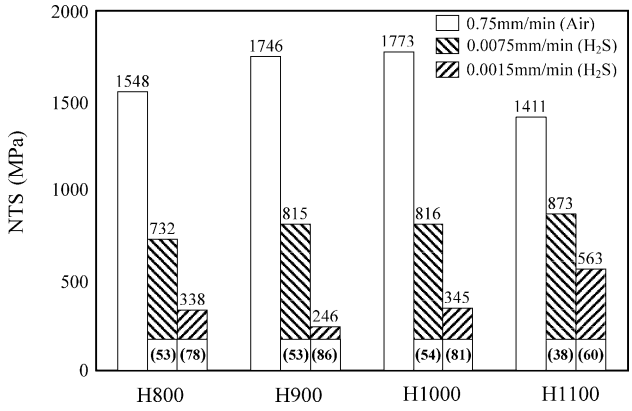

Fig. 3. Notched tensile strength (NTS) of aged PH 13-8 Mo specimens tested in saturated H_2S solution and laboratory air. Note that the percentage within parentheses indicates the NTS loss in H_2S.

specimen exhibited the highest NTS, while the H800 specimen had the lowest NTS among the specimens. The effect of hydrogen embrittlement was reflected by NTS loss of the specimens. The lower susceptibility to SSCC of the H1100 specimen as compared to other specimens was associated with the extensive formation of reverted austenite. The decrease in displacement rates, i.e. prolonged interaction time between the specimen and hydrogen, revealed the same tendency except an increased NTS loss for a given specimen. In notched specimens, the plastic zone size ahead of notch front was similar for specimens aged to the same strength level. Suppose the same critical hydrogen concentration is required to induce cracking in the plastic zone. Then, the susceptibility to hydrogen embrittlement of the material can be directly related to hydrogen permeation properties, which are discussed in the next section.

3.3. Hydrogen permeation

Table 2 lists the permeation results including effective hydrogen diffusivity (D_{eff}), permeation flux ($J_\infty L$), and apparent hydrogen solubility (C_{app}) of various specimens. It was reported that hydrogen permeation properties could be related to the microstructures of the material [12–14]. Xu [13] reported that dislocations (reversible traps) are the dominant trapping sites for hydrogen in a low carbon martensite. It is known that the C_{app} is dependent on the amount and nature of trapping sites that includes irreversible (strong) and reversible (weak) traps in the specimen. Increasing the aging temperature of PH 13-8 Mo steel, a significant decrease in dislocation density [2] and an increase in reverted austenite (irreversible traps) [2,3] are found. It is reported [11] that the density of β-NiAl precipitates is in the same order of $10^{24}\,m^{-3}$ for the alloy aged in the temperature range of 510–550 °C and decreases to $10^{23}\,m^{-3}$ for 620 °C aged specimen. In addition, the particle size of β-NiAl is about 3–6 nm and resistant to growth in the aging temperature between 450–620 °C [11]. Apparently, the amount of irreversible traps, i.e. reverted austenite, was highest in the H1100 specimen and lowest in the H800 specimen. As a result, irreversible traps

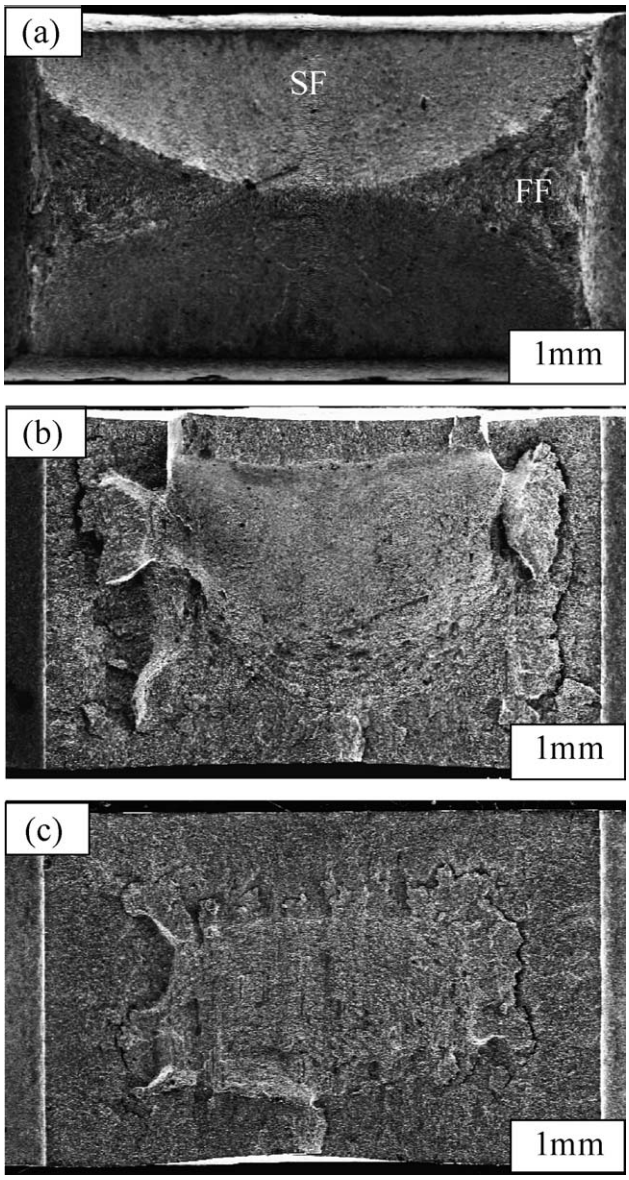

Fig. 4. Macrographs showing the fracture appearance of the H1100 specimen tested in (a) air, (b) saturated H_2S solution at a displacement rate of 0.0075 mm/min, and (c) saturated H_2S solution at a displacement rate of 0.0015 mm/min.

Table 2
Permeation properties of PH 13-8 Mo specimens aged at various temperatures

	H800	H900	H1000	H1100
D_{eff} ($m^2\,s^{-1}$)	2.44×10^{-12}	2.40×10^{-12}	2.20×10^{-12}	2.48×10^{-13}
$J_\infty L$ (mol (H) $s^{-1}\,m^{-1}$)	1.1×10^{-9}	1.19×10^{-9}	1.16×10^{-9}	7.35×10^{-10}
C_{app} (mol (H) m^{-3})	450	500	530	2960

increased at the expense of reversible traps as the aging temperature rose. Permeation results indicated that the H800, H900 and H1000 specimens had nearly the same permeability, but H1100 specimen had a much lower diffusivity and higher solubility than other specimens.

Dislocations and coherent precipitates are known to be weak hydrogen traps, in contrast, reverted austenite is considered to be a strong trap. Reverted austenite could absorb hydrogen at interfaces or within itself. The number of trapping sites, which were predominantly reversible traps for H800, H900 and H1000 specimens was about the same. The lack of strong traps in these specimens resulted in analogous hydrogen diffusivity and solubility in permeation measurements. In case of the H1100 specimen, D_{eff} about one order less and C_{app} about six times higher as compared with other specimens were noticed. The great increase in the amount of reverted austenite in the over-aged specimen accounted for such consequences. Moreover, the increase in strong traps of the H1100 specimen was also responsible for a significant retardation of hydrogen diffusivity and a low hydrogen flux.

The diffusion of hydrogen depends not only on moving down the concentration gradient but also on moving toward the locations with high hydrostatic stresses [15–17]. Since crack or notch causes locally triaxial stresses ahead of it, increasing the stress concentration makes hydrogen become more aggressive as an embrittling agent [18,19]. Permeation results implied that less amount of reverted austenite in the specimens aged below 538 °C allowed rapid diffusion of hydrogen to the stress concentrator, resulting in a high susceptibility to hydrogen embrittlement as shown in Fig. 3. Moreover, coherent precipitation of fine β-NiAl particles within the matrix also meant dislocations will cut those fine precipitates, leading to the high susceptibility to SSCC for specimens aged below 538 °C.

Pressouyre [20] reported that irreversible traps help in delaying the onset of hydrogen-induced cracking. A high specific amount of strong hydrogen traps is thought to be beneficial to resist hydrogen embrittlement [21]. While in Pound's study [22], irreversible trapping constants which link to the density of irreversible traps in the material are proportional to the susceptibility of materials [22]. The results of present work were in agreement with the Pressouyre's study. The difference between studies of Pressouyre [20] and Pond [22] would be attributed to the nature of irreversible traps. The beneficial traps such as austenite could trap and impede the hydrogen diffusion inward hence helped to reduce cracking susceptibility. Consequently, the more reverted austenite in the over-aged specimen the less susceptible to hydrogen embrittlement would be the result. Alternatively, the accumulation of hydrogen at the interfaces between matrix and inclusions led to interfacial separations, resulting in an increased susceptibility of the alloy [23–25].

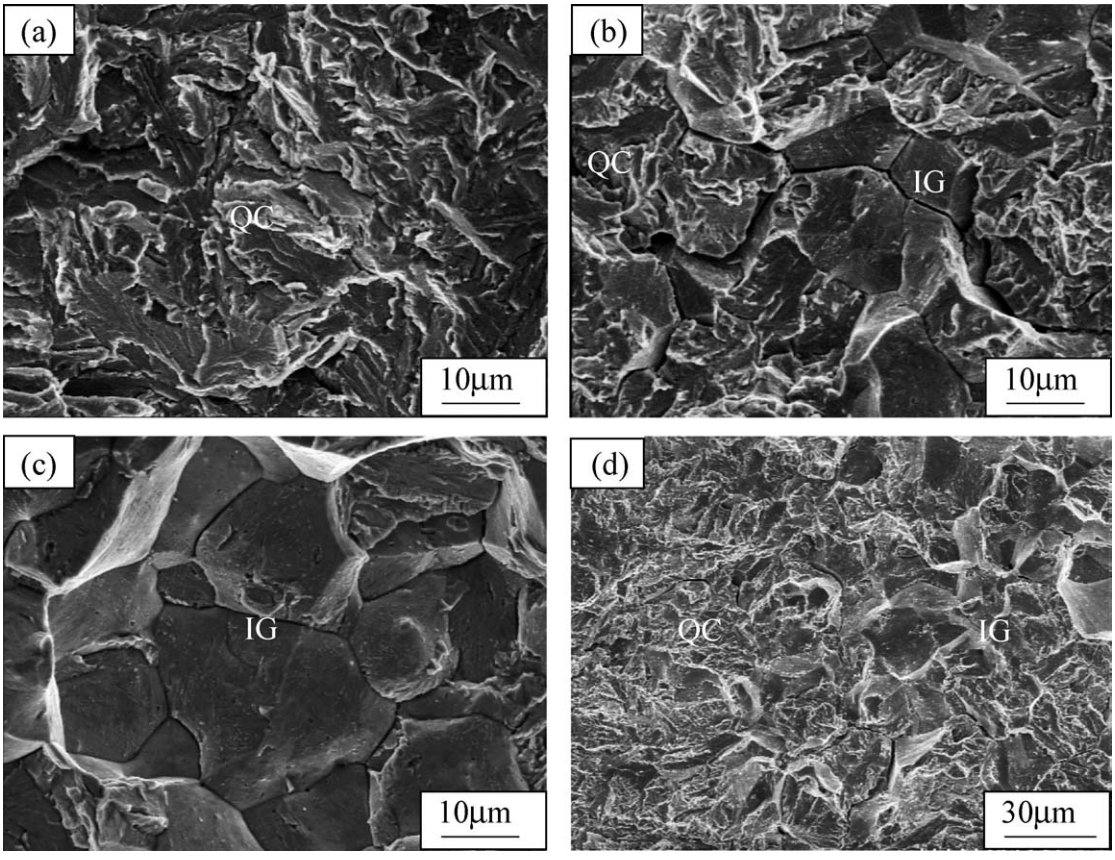

Fig. 5. SEM fractographs of the specimens tested in the saturated H_2S solution: (a) quasi-cleavage (QC) fracture in the H800 specimen; (b) QC mixed with intergranular (IG) fracture in the H1100 specimen tested at the displacement rate of 0.0075 mm/min; (c) mainly IG fracture in the H1100 specimen tested at the displacement rate of 0.0015 mm/min; and (d) the change of fracture mode in the H1100 specimen from IG to QC before final fast fracture regardless of displacement rates.

3.4. Fracture morphology

Fig. 4(a) is a typical fracture appearance of the H1100 specimen after notched tensile tests in air, in which consisted of slant fracture (SF) and flat fracture (FF) ahead of notch fronts. In fact, all aged specimens in air exhibited nearly the same macroscopic fracture appearance and the fracture surface revealed a ductile dimple fracture. For specimens tested in the saturated H_2S solution, an obvious change in macroscopic fracture morphology was found. Except for the fast fracture region associated with overloading, predominantly FF with secondary cracks on the fracture surface was observed as displayed in Fig. 4(b). The changes in macroscopic fracture morphology also reflected the detrimental effect of hydrogen embrittlement. For instance, the embrittled area of the H1100 specimen increased as the displacement rate reduced to 0.0015 mm/min (Fig. 4(c)). The corresponding NTS loss was 60% as compared with 38% of the same specimen tested at 0.0075 mm/min displacement rate.

SEM fractographs of aged specimens tested in the saturated H_2S solution are shown in Fig. 5. Quasi-cleavage fracture (Fig. 5(a)) was observed for the specimens aged below 538 °C, regardless of displacement rates. It was deduced that a homogeneous distribution of hydrogen traps for specimens aged below 538 °C exhibited quasi-cleavage fracture testing in the saturated H_2S solution. Furthermore, it was found that intergranular cracking inter-dispersed in quasi-cleavage fracture was present in the H1100 over-aged specimen (Fig. 5(b)) and the extent of intergranular fracture increased greatly at a slower displacement rate (Fig. 5(c)). It was worth mentioning that a change in fracture modes from intergranular to quasi-cleavage (Fig. 5(d)) occurred as the crack propagated into the interior before final dimple fracture. The short-time interaction of hydrogen with materials caused a reduced damage at grain boundaries under high crack growth rate. Consequently, quasi-cleavage fracture was observed in the region experiencing a fast subcritical crack growth before final fracture in the H1100 specimen. It was expected that the presence of some grain boundary austenite in the H1100 specimen could trap more hydrogen therein, resulting in intergranular separations eventually. Lowering the displacement rate would certainly enhance the hydrogen-metal interaction in the test. The accumulation of hydrogen along grain boundaries was more significant in the H1100 specimen, which would lead to severe intergranular cracking as revealed by comparing Fig. 5(b) with (c).

4. Conclusions

1. PH 13-8 Mo specimens aged below 538 °C had nearly same permeation properties. However, the specimen aged at 593 °C (H1100) exhibited significantly lower diffusivity and higher solubility of hydrogen. The more reverted austenite (irreversible hydrogen traps) in the over-aged material would account for such characteristics.
2. PH 13-8 Mo steel was susceptible to sulfide stress corrosion cracking. For the specimens aged below 538 °C, similar permeation properties led to roughly the same susceptibility to hydrogen embrittlement. The H1100 specimen with much lower diffusivity and hydrogen flux resulted in a less NTS loss as compared to other aged specimens.
3. The trapping of hydrogen in the matensite matrix enhanced the quasi-cleavage fracture for the specimens aged below 538 °C. In addition, the presence of some grain boundary austenite in the H1100 specimen could trap hydrogen therein, leading to intergranular separations after notched tensile tests in the saturated H_2S solution.

References

[1] V. Seetharaman, M. Sundararaman, R. Krishnan, Mater. Sci. Eng. 47 (1) (1981) 1–11.
[2] P.W. Hochandel, C.V. Robino, G.R. Edwards, M.J. Cieslak, Metall. Trans. 25A (4) (1994) 789–798.
[3] P. Munn, B. Andersson, Corrosion 46 (4) (1990) 286–295.
[4] P.W. Hochanadel, C.V. Robino, G.R. Edwards, M.J. Cieslak, Metall. Trans. 25A (4) (1994) 697–704.
[5] G.T. Murry, H.H. Honegger, T. mousel, Corrosion 40 (4) (1984) 146–151.
[6] L.M. Young, M.R. Eggleston, H.D. Solomon, L.R. Kaisand, Mater. Sci. Eng. A203 (1–2) (1995) 377–387.
[7] J.R. Scully, M.J. Cieslak, J.A. Van Den Avyle, Scripta Met. 31 (2) (1994) 125–130.
[8] R.R. Gaugh, Mater. Perf. 16 (9) (1977) 24–29.
[9] M.A. Devanathan, Z. Stachurski, Proc Roy Soc (London) A270 (1962) 90–102.
[10] A. Turnbull, R.B. Hutchings, Mater. Sci. Eng. A177 (1994) 161–171.
[11] D.H. Ping, M. Ohnuma, Y. Hirakawa, Y. Kadoya, K. Hono, Mater. Sci. Eng. A 394 (2005) 285–295.
[12] R. Valentini, A. Solina, Mater. Sci. Tech. 10 (10) (1994) 908–914.
[13] J. Xu, X.Z. Yuan, X.K. Sun, B.M. Wei, Scripta Met. 29 (1993) 925–930.
[14] N. Parvathavarthini, S. Saroja, R.K. Dayal, J. Nuclear Mater. 264 (1999) 35–47.
[15] J. Toribio, A.M. Lancha, M. Elices, Mater. Sci. Eng. A145 (2) (1991) 167–177.
[16] J. Toribio, J. Mater. Sci. 28 (9) (1993) 2289–2298.
[17] A.T. Yokobori Jr., T. Nemoto, K. Satoh, T. Yamada, Eng. Fract. Mech. 55 (1) (1996) 47–60.
[18] D. Hardie, S. Liu, Corr. Sci. 38 (5) (1996) 721–733.
[19] S. Liu, Z. Ziyong, Ke Wei, J. Mater. Sci. Tech. 12 (1) (1996) 51–56.
[20] G.M. Pressouyre, I.M. Bernstein, Acta Metall. 27 (1) (1979) 89–100.
[21] G.M. Pressouyre, I.M. Bernstein, Metall. Trans. 9A (11) (1978) 1571–1580.
[22] B.G. Pound, Acta Metall. Mater. 38 (12) (1990) 2373–2381.
[23] T. Taira, K. Tsukada, Y. Koyashi, H. Inagaki, T. Watanabe, Corrosion 37 (1) (1981) 5–16.
[24] A. Chavane, M. Habashi, G.M. Pressouyre, J. Galland, Corrosion 42 (1) (1986) 54–61.
[25] M. Kimura, N. Totsuka, K. Amano, J. Matsuyama, Y. Nakai, Corrosion 45 (4) (1989) 340–346.